ACCSCIENCE PUBLISHING

Journal of Seismic Exploration

ARTICLE

A fluid factor inversion method using the frequency-domain two-step sub-band regularization

Peng Zhang[1], Ying Xiao[1], Peng Xiao[2,3]*, Pang Chen[1], and Wangyang Xu[3]

[1]Geophysical R&D Institute, Geophysical-COSL, China Oilfield Services Ltd., Tianjin, China

[2]Sichuan Energy Investment Group Co., Ltd., Chengdu, Sichuan, China

[3]Reservoir Geophysics Laboratory, School of Geoscience and Technology, Southwest Petroleum University, Chengdu, Sichuan, China

Abstract

In oil and gas seismic exploration, fluid factors are key parameters for identifying reservoir fluid properties and evaluating reservoir potential. Although regularization methods are commonly used to enhance inversion stability, traditional time–domain lateral constraint methods struggle to effectively address the issue of abrupt lateral stratigraphic variations. This paper aims to improve the prediction accuracy and stability of fluid factors in such scenarios. Based on the characteristic that frequency-domain seismic data exhibit stronger correlation during stratigraphic abrupt changes, this paper proposes a frequency-domain two-step sub-band regularization inversion method. First, a difference operator is introduced into the frequency domain to construct the objective function, and the Alternating Direction Method of Multipliers algorithm is adopted as the solution. Furthermore, a two-step sub-band regularization strategy is proposed: First, integrating low-frequency and high-frequency residual terms into the same objective function; then performing inversion in two stages. These stages first use low-frequency data inversion to obtain the general profile of the subsurface structure as an initial model, followed by using high-frequency data inversion based on this to obtain detailed information. Theoretical model tests have verified the superiority of this method under complex geological conditions. Field application in practical work areas shows that the frequency-domain two-step method significantly outperforms the traditional time–domain lateral constraint L1 regularization method in terms of vertical resolution and lateral continuity. This method provides a more accurate and stable solution for fluid identification under complex geological conditions.

Keywords: Frequency-domain regularization; Fluid factor; Lateral constraint; Alternating Direction Method of Multipliers; Pre-stack inversion

***Corresponding author:**
Peng Xiao
(15680819559@163.com)

Citation: Zhang P, Xiao Y, Xiao P, Chen P, Xu W. A fluid factor inversion method using the frequency-domain two-step sub-band regularization. *J Seismic Explor*. 2025;34(5):1-17. doi: 10.36922/JSE025310048

Received: July 28, 2025

1st revised: August 22, 2025

2nd revised: September 1, 2025

3rd revised: September 16, 2025

4th revised: September 23, 2025

Accepted: October 11, 2025

Published online: October 30, 2025

1. Introduction

The accurate identification of subsurface fluids is crucial for oil and gas exploration and development. It enables geologists and engineers to gain a deeper understanding of reservoir characteristics, predict the distribution of oil and gas reservoirs, and thereby

improve the success rate of exploration and development efficiency. As a result, research on fluid factors has become a key and dynamic research direction. Initially, fluid factors were parameters constructed based on variations in P-wave and S-wave velocities, used to detect hydrocarbon anomalies in reservoirs. Over time, researchers have not only developed multi-parameter methods and innovated direct extraction techniques, but also clarified the petrophysical significance of fluid factors and applied them to the exploration of unconventional oil and gas resources. The concept of fluid factor was first proposed by Smith and Gidlow[1] in 1987, originally referring to a parameter constructed by the weighted difference operation of relative variations in P-wave and S-wave velocities.[1] Goodway *et al.*[2] proposed the Lame's Modulus and Density technique, the core of which lies in using P-wave and S-wave velocity information from seismic data to invert for rock Lame parameters.[2] These parameters can provide more direct petrophysical property information than traditional P-wave and S-wave velocities, thereby enabling more effective identification of reservoir fluids and lithology. Patrick Connolly[3] proposed the concept of elastic impedance, which extended fluid identification research from the reflection coefficient domain to the impedance domain, significantly improving the accuracy and efficiency of reservoir fluid identification using seismic data.[3] In 2003, George Smith[4] proposed two fluid factor concepts: the fluid factor angle and the crossplot angle. Based on pre-stack amplitude versus offset (AVO) analysis, these concepts identify pore fluids by calculating angles related to fluid factors and crossplots.[4] To address the challenge that AVO responses in carbonate reservoirs are weaker than those in clastic reservoirs—making it difficult to accurately determine fluid properties—Peng *et al.*[5] proposed an innovative multi-angle elastic impedance fluid identification method.[5] Zheng *et al.*[6] constructed a new fluid factor formula based on fluid factors and Poisson impedance, which improves the sensitivity of fluid identification and lithology prediction.[6] Zong *et al.*[7] proposed a simultaneous inversion method named Fluid Factor, Mu (shear modulus), Rho (density)-Amplitude Variation with Angle based on partial angle stack seismic gather. This method is applicable for direct inversion of fluid factors, shear modulus, and density in heterogeneous reservoirs.[7] Yin *et al.*[8] summarized the key scientific issues in seismic fluid identification, focusing on reviewing the main progress of rock physics-driven seismic fluid identification, and discussed the related opportunities, challenges, and future research directions in seismic fluid identification.[8] Li *et al.*[9] derived a two-term approximate seismic reflection coefficient equation containing Gassmann fluid and shear modulus terms, based on Zoeppritz equation approximation and petrophysical relationships of elastic parameters. Under the Bayesian inversion framework, they developed a probabilistic pre-stack inversion method, using this equation, that excludes large-angle seismic data for direct inversion of the Gassmann fluid term and reservoir fluid identification[9] Jiang *et al.*[10] proposed to simplify the bulk modulus of saturated rocks using fluid bulk modulus and porosity, derived the linearized P-wave reflection coefficient as a function of fluid bulk modulus and modified porosity, and then established an inversion method to estimate fluid bulk modulus and porosity from observed seismic data using the obtained reflection coefficients and elastic impedance.[10] Liu *et al.*[11] proposed a new fluid factor by adding a correct term to the J attribute, and based on the neural network model, used deep learning methods to train and predict this new fluid factor.[11] In 2020, Li and Yin[12] proposed a mixed probability model-driven pre-stack seismic inversion method, providing a new technical approach for fluid factor extraction.[12] Farfour and Castagna *et al.*[13] introduced a new expression for fluid factors commonly used in AVO analysis and interpretation. The expression is a function of the common AVO intercept, gradient, and a weighting coefficient, which can be used to suppress the influence of lithology and other factors unrelated to fluid content.[13] Wu *et al.*[14] conducted joint inversion of fluid factor and brittleness index based on pre-stack seismic records from typical coal-measure gas blocks in the Sichuan Basin.[14] Lin *et al.*[15] first proposed a new method that treats the dynamic vertical reflectivity series as a dynamic variable varying with depth and lithology, and applied it to fluid factor calculation and inversion.[15] Zhang *et al.*[16] explored the concept of Q elastic impedance fluid factor and established a quantitative relationship between elastic impedance and Q elastic fluid factor for reservoir fluid identification.[16] Pan *et al.*[17] proposed an inversion method based on the elastic impedance of vertically transverse isotropic media, which can reasonably and accurately predict the fluid factor, Young's modulus, and anisotropic parameters, providing a new approach for fluid identification in shale reservoirs, prediction of brittleness parameters, and assessment of the development degree of anisotropy.[17]

Second, regularization inversion methods are crucial for improving the accuracy and reliability of subsurface fluid factor identification. They can suppress noise and instability by introducing constraints during the inversion process, enhancing the continuity and physical interpretability of inversion results. The concept of regularization was first proposed by Andrey Tikhonov[18] in 1943, and Tikhonov further developed the Tikhonov regularization method in 1963.[19] In 1992, Rudin *et al.* proposed the total variation regularization method for image denoising, particularly in scenarios affected by

additive white Gaussian noise.[20] In 2005, Zou and Hastie[21] proposed the elastic net regularization, also known as L1+L2 regularization. Gholami[22] proposed an innovative nonlinear multichannel impedance inversion technique, which employs a total variation regularization strategy to guide the inversion process, promoting blocky features in the solutions. This method effectively highlights the boundaries of geological bodies and reduces random local inhomogeneities in data.[22] Ruixue *et al.*[23] proposed an innovative two-parameter shaping regularization method, which integrates the advantages of Tikhonov regularization and Total variation regularization. In 2016, Mousavi and Langston[24] presented a hybrid seismic denoising method in their research, combining higher-order statistics with an improved wavelet block thresholding technique. This method enhances denoising accuracy and efficiency while preserving effective signals in seismic data. Aiming at the issue that regularization constraints ignore the amplitude information of stratigraphic boundaries, Pan *et al.*[25] proposed an anisotropic total variation regularization with Lp-norm minimization (ATpV) pre-stack three-parameter inversion method based on reweighted L1. For the 1st time, this method integrates the reweighted L1 approach with the ATpV method and introduces it into pre-stack inversion, effectively restoring the sparsity of inversion results and improving inversion accuracy.[25]

This paper proposes a fluid factor inversion method based on frequency-domain two-step sub-band regularization, mainly embodied in the integration of regularization methods with multi-channel inversion theory in the frequency domain. It innovatively presents a frequency-domain lateral constraint regularization inversion method and further extends it. On this basis, aiming at the characteristics of seismic data, a two-step sub-band regularization method is proposed. The two-step sub-band regularization method first uses low-frequency band inversion to obtain the general morphology of subsurface structures, then performs high-frequency band inversion based on this model to acquire detailed geological details. Theoretical model verification shows that it processes low-frequency and high-frequency information more delicately, with significantly improved accuracy and noise resistance. Overall, compared with the traditional time–domain regularization multi-channel inversion method, it can provide more accurate inversion results during abrupt changes in subsurface media.

2. Methodology

2.1. The reflection coefficient equation incorporating the fluid factor

Wang *et al.*[26] clearly pointed out that the fluid factor, defined as the ratio of Lame coefficients to shear modulus (λ/μ)., exhibits higher sensitivity to fluid properties and lower sensitivity to porosity compared with other fluid factors. This characteristic enables effective differentiation between oil and water layers, enhancing the success rate of hydrocarbon detection. Therefore, this paper uses the ratio of Lame coefficients to shear modulus (λ/μ) as the fluid factor for inversion research in subsequent sections. Consequently, the GRAY formula involving these two parameters is introduced to derive the reflection coefficient equation incorporating the fluid factor. It should be noted that when facing geological bodies with high impedance contrast, the inversion accuracy of the GARY approximation will decrease with the increase of the incident angle. Therefore, the angle of multi-angle seismic data used for inversion should not be too large. The basic dimensions of seismic data are defined as follows: M is the number of incident angles, N is the number of seismic traces, and T is the number of sampling points per trace. The logarithmic vectors of the core parameters, namely the fluid factor λ/μ., shear modulus μ., and density ρ., are $L_{\lambda/\mu.}$, $L_{\mu.}$, and $L_{\rho.}$, respectively, (all are $T\times N$ matrices). All matrix dimensions involved in this paper are determined based on this basic dimensional framework.

The GRAY approximation is as follows in **Equation (I)**:

$$R(\theta)=(\frac{1}{4}-\frac{1}{2}k^2)sec^2\theta\frac{\Delta\lambda}{\lambda}+k^2(\frac{1}{2}sec^2\theta-2sin^2\theta)\frac{\Delta\mu}{\mu}+(\frac{1}{2}-\frac{1}{4}sec^2\theta)\frac{\Delta\rho}{\rho} \quad \text{(I)}$$

where, θ is the incident angle, in degrees; λ is the Lame coefficient; μ is the shear modulus, in Pa; ρ is the density, $k = V_s/V_p$ is the ratio of S-wave to P-wave velocity; $R_{\lambda} = \Delta\lambda/\lambda$ is the λ .reflection coefficient; $R_{\mu} = \Delta\mu/\mu$ is the μ.reflection coefficient; and $R_{\rho} = \Delta\rho/\rho$ is the density reflection coefficient.

Derivation with respect to λ/μ gives **Equation (II)**:

$$d(\lambda/\mu)=d(\lambda)\frac{\partial(\lambda/\mu)}{\partial\lambda}+d(\mu)\frac{\partial(\lambda/\mu)}{\partial\mu} \quad \text{(II)}$$

Dividing both sides of **Equation (II)** by λ/μ gives **Equations (III)** and **(IV)**:

$$\frac{d(\lambda/\mu)}{\lambda/\mu}=\frac{d(\lambda)\frac{\partial(\lambda/\mu)}{\partial\lambda}}{\lambda/\mu}+\frac{d(\mu)\frac{\partial(\lambda/\mu)}{\partial\mu}}{\lambda/\mu}=\frac{d(\lambda)}{\lambda}-\frac{d(\mu)}{\mu} \quad \text{(III)}$$

$$\frac{\Delta(\lambda/\mu)}{\lambda/\mu}=\frac{\Delta(\lambda)}{\lambda}-\frac{\Delta(\mu)}{\mu} \quad \text{(IV)}$$

Substituting **Equation (IV)** into **Equation (I)** and simplifying them yields **Equation (V)**:

$$R(\theta) = (\frac{1}{4} - \frac{1}{2}k^2)sec^2\theta \frac{\Delta(\lambda/\mu)}{\lambda/\mu} + (\frac{1}{4}sec^2\theta - 2k^2sin^2\theta) \frac{\Delta\mu}{\mu} + (\frac{1}{2} - \frac{1}{4}sec^2\theta)\frac{\Delta\rho}{\rho} = a(\theta)R_{\_\lambda/\mu} + b(\theta)R_{\_\mu} + c(\theta)R_{\_\rho} = a(\theta)R_{\_\lambda/\mu} + b(\theta)R_{\_\mu} + c(\theta)R_{\_\rho} \quad (V)$$

Where $R_{\_\lambda/\mu}$ represents the fluid factor λ/μ reflection coefficient. **Equation (V)** establishes a direct linear relationship among the λ/μ reflection coefficient, μ reflection coefficient, density reflection coefficient, and P-P reflection coefficient. Next, the objective function for the fluid factor λ/μ is constructed through **Equation (V)**. First, by establishing the relationship between seismic data and the parameters to be inverted through the reflection coefficient equation, we can obtain **Equation (VI)**:

$$S = AL \quad (VI)$$

Where S .is the multi-angle seismic data volume, L is the model parameter, and A is the forward operator.

2.2. The principle of the two-step sub-band regularization method

Based on the forward modeling of **Equation (VI)** derived from the above transformations, the traditional objective function is expressed as **Equation (VII)**:

$$J(L) = \min_L AL - S_2^2 \quad (VII)$$

Where $\|.\|_2^2$ is the L2 norm. By incorporating the initial model L_0 into the objective function, the constraint of the initial model term is realized. Finally, by adding the time–domain L1 regularization method to the objective function, the objective function of the time–domain L1 regularization method can be expressed as **Equation (VIII)**:

$$J(L) = \min_L AL - S_2^2 + \mu_{reg}L - L_{02}^2 + \lambda_{reg}L_1 \quad (VIII)$$

Considering the strong correlation between adjacent seismic traces, the difference operator *D* is introduced. The time–domain horizontal constraint L1 regularization method adds an additional horizontal constraint term *D* based on **Equation VIII**. Thus, the objective function of the time-domain horizontal constraint L1 regularization inversion method is presented as **Equation (IX)**:

$$J(L) = \min_L AL - S_2^2 + \mu_{reg}L - L_{02}^2 + \lambda_{reg}DL_1 \quad (IX)$$

Where μ_{reg} is the regularization parameter for the initial model, the initial model L_0 is typically obtained by smoothing logging data, λ_{reg} is the regularization factor, and $\|\cdot\|_1$ is the L1 norm.

When abrupt changes occur in the stratum structure, the limitations of the time–domain horizontal constraint method become significantly prominent. Therefore, the inversion algorithm is extended to the frequency domain. Time domain signals are a combination of high and low frequencies, with low correlation between adjacent data. The residual of the differential operator *D* is susceptible to "frequency confusion errors," where horizontal constraints make it difficult to distinguish real geological changes from noise interference, leading to misjudgment of formation mutations and noise. After frequency band division, the correlation between data within the same frequency band is significantly enhanced, which can accurately distinguish geological mutations and interference. The frequency-domain regularization method achieves efficient conversion between the time–frequency domains by introducing the Fourier transform matrix *F* Substituting this matrix into the objective function, the objective function expression of the frequency-domain L1 horizontal constraint regularization inversion method is constructed as follows in **Equation (X)**:

$$J(L) = \min_L FAL - FS_2^2 + \mu_{reg}FL - FL_{02}^2 + \lambda_{reg}DFL_1 \quad (X)$$

Based on the difference in information contained in the low-frequency and high-frequency bands of seismic data, this paper innovatively proposes a two-step sub-band regularization inversion method within the framework of the frequency-domain L1 regularization inversion method. In the two-step method, the objective function is clearly divided into two independent parts, which respectively process the seismic data in the low-frequency and high-frequency bands. When processing data, the main frequency of seismic data is first obtained through spectral analysis. Then, the seismic data is divided into low-frequency and high-frequency parts by setting high-frequency and low-frequency limits. To avoid significant frequency truncation errors, modules and filters from mature commercial software can be directly used. First, an objective function with low-frequency seismic data is constructed, and the low-frequency band model L_{low}.is inverted by relying on the low-frequency seismic data S_{low}. (**Equation [XI]**):

$$J(L_{low}) = \min_L FAL - FS_{low2}^2 + \mu_{reg}FL - FL_{02}^2 + \lambda_{reg}DFL_1 \quad (XI)$$

Finally, the obtained low-frequency band model L_{low}. is incorporated into the initial model constraint term to replace L_0, and when combined with high-frequency seismic data, the objective function for the second stage can be obtained as **Equation (XII)**:

$$J(L) = \min_L FAL - FS_{high2}^2 + \mu_{reg}FL - FL_{low2}^2 + \lambda_{reg}DFL_1 \quad (XII)$$

Where F denotes the Fourier transform matrix, S_{low} denotes the seismic data in the low-frequency part, and S_{high} denotes the seismic data in the high-frequency part. The Fourier transform itself is a global transform, but combined with the proposed two-step sub-band regularization, it can achieve local constraints in the frequency domain, which is a mathematical advantage that cannot be achieved in the time domain.

Finally, to solve the two-step sub-band regularization inversion method, a matrix R_{low} is first introduced to make it equal to *DFL* .in **Equation (XII)**. Then, a quadratic penalty term and a dual term are added to transform **Equation (XII)** into an unconstrained optimization problem:

$$J(L_{low}) = \min_{L} FAL - FS_{low2}^{2} + \mu_{reg} FL - FL_{02}^{2} + \lambda_{reg} R_{low1} + \eta R_{low} - DFL + C_{low2}^{2} \quad \text{(XIII)}$$

Similarly, using the same transformation method, **Equation (XIII)** can be converted into the following unconstrained problem in **Equation (XIV)**:

$$J(L) = \min_{L} FAL - FS_{high2}^{2} + \mu_{reg} FL - FL_{low2}^{2} + \lambda_{reg} R_{high1} + \eta R_{high} - DFL + C_{high2}^{2} \quad \text{(XIV)}$$

It should be noted that the selection of parameters relies on multiple experiments to select empirical values. Among them are μ_{reg}=0.005–0.02, λ_{reg}=0.01–0.04, and η = 0.001–0.01. In the selection of the L1 regularization parameter λ_{reg}, a larger value should be set in the low-frequency range to strengthen constraints and ensure the overall continuity of the formation, while a smaller value should be set in the high-frequency range to weaken constraints and preserve the details of geological changes. An example of the impact of μ_{reg} and λ_{reg} on the inversion results can be found in the Appendix. Usually, within a given reference range, the inversion error increases with the increase of μ_{reg} and decreases with the rise in λ_{reg}. Among them, the influence of u on the inversion results is relatively small, less than the influence of r on the inversion results.

Then, using the alternating direction method of multipliers algorithm and combining **Equations (XIII)** and **(XIV)**, it is decomposed into the following subproblems (**Equations [XV]–[XX]**):

$$J(L_{low}) = \min_{L} FAL - FS_{low2}^{2} + \mu_{reg} FL - FL_{02}^{2} + \eta R_{low} - DFL + C_{low2}^{2} \quad \text{(XV)}$$

$$J(L) = \min_{L} FAL - FS_{high2}^{2} + \mu_{reg} FL - FL_{low2}^{2} + \eta R_{high} - DFL + C_{high2}^{2} \quad \text{(XVI)}$$

$$J(R_{low}) = \lambda_{reg} R_{low1} + \eta R_{low} - DFL + C_{low2}^{2} \quad \text{(XVII)}$$

$$J(R_{high}) = \lambda_{reg} R_{high1} + \eta R_{high} - DFL + C_{high2}^{2} \quad \text{(XVIII)}$$

$$J(C_{low}) = \eta R_{low} - DFL + C_{low2}^{2} \quad \text{(IX)}$$

$$J(C_{high}) = \eta R_{high} - DFL + C_{high2}^{2} \quad \text{(XX)}$$

Finally, the above subfunctions are solved. The workflow of the two-step sub-band regularization method in the frequency domain is shown in Figure 1.

3. Results

3.1. Synthetic data testing

To verify the inversion performance of the method, a fragment of the Marmousi2 model was selected to demonstrate the inversion effect, as shown in Figure 2. The model contained 5,000 traces horizontally, with 2,000 sampling points per trace. Based on the Marmousi2 theoretical model, reflection coefficients at three different incident angles (10°, 20°, and 30°) were calculated, which were then convolved with a zero-phase wavelet with a dominant frequency of 30 Hz to synthesize multi-angle seismic data volumes. Figure 3 shows the angular seismic data volumes corresponding to these three incident angles (10°, 20°, and 30°), respectively.

Next, the traditional time–domain horizontal constraint L1 regularization method and the proposed two-step sub-band regularization method were applied to a two-dimensional model. As shown in Figure 4, the inversion results of the ratio of Lame coefficient to shear modulus obtained by the time-domain L1 regularization and time–domain horizontal constraint L1 regularization methods are displayed.

To more intuitively compare the inversion effects of the two methods, as shown in Figure 5, the inversion errors for each method were calculated by measuring the differences between the original model and the results of the two inversion methods.

From the images in the red box of Figure 5, it can be seen that the area of bright regions in Figure 5B is smaller than that in Figure 5A, and the light blue line to the left of the red box in Figure 5B is thinner than the line at the same position in Figure 5A. This indicates that the error of the two-step sub-band regularization method is lower than that of the time–domain L1 horizontal constraint regularization method, suggesting that the two-step sub-band regularization method outperforms the time–domain L1 horizontal constraint regularization method in inverting fluid factors. This difference is

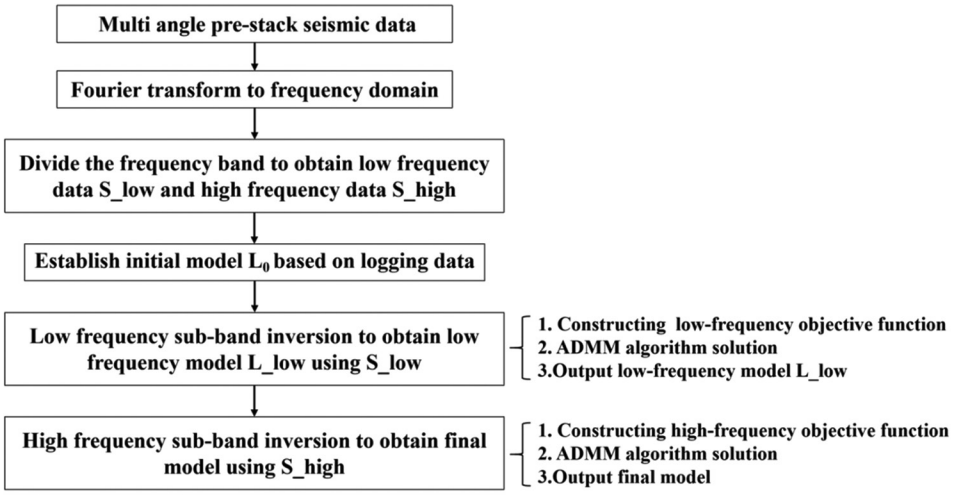

Figure 1. Workflow diagram of the two-step sub-band regularization inversion
Abbreviation: ADMM: Alternating direction method of multipliers.

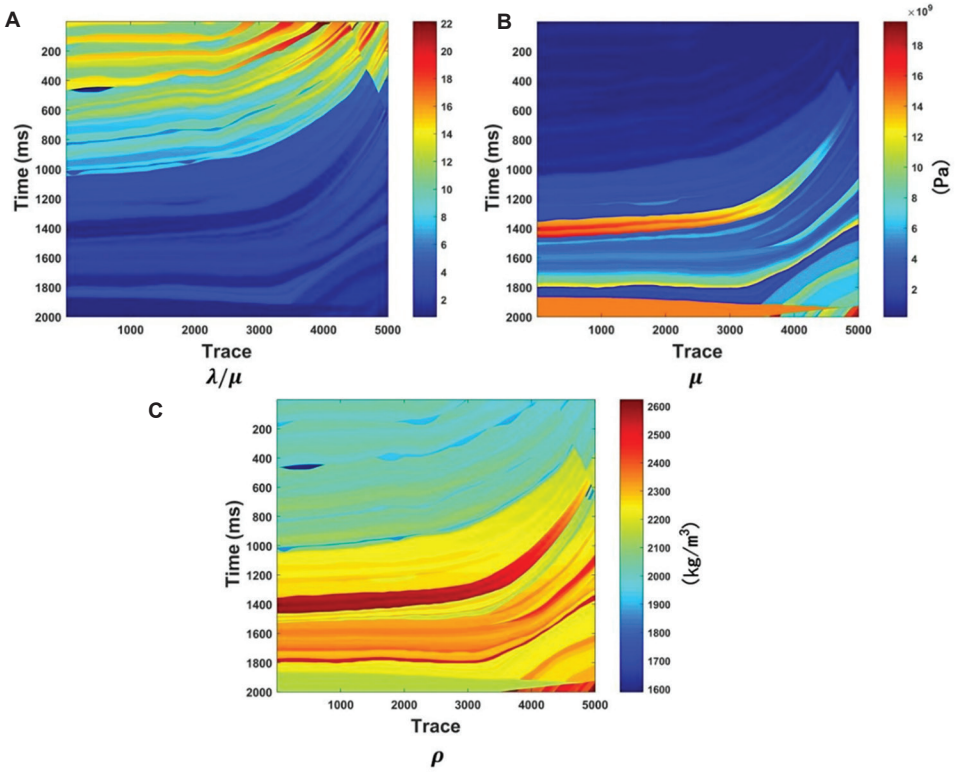

Figure 2. Theoretical model. (A) Ratio of Lame coefficient to shear modulus; (B) shear modulus; and (C) density,

attributed to the more refined sub-band processing and optimization of the two-step method, which more effectively reduces errors and improves inversion accuracy.

Furthermore, Figures 6 and 7 also show the error images of the inversion results for shear modulus and density using the two regularization methods. In terms of the overall inversion error, the sub-band regularization method exhibited lower errors than the time-domain L1 horizontal constraint regularization method, demonstrating the effectiveness of the sub-band regularization method.

To demonstrate the effects and differences between the time–domain L1 horizontal constraint regularization

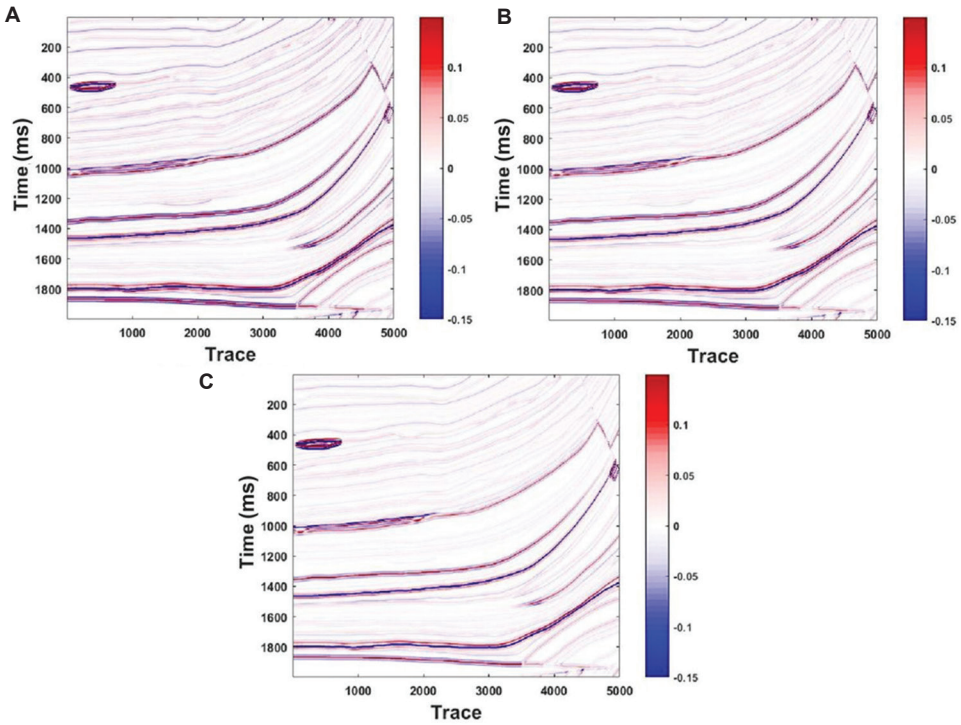

Figure 3. Synthetic seismic records at different incident angles. (A) 10°; (B) 20°; and (C) 30°.

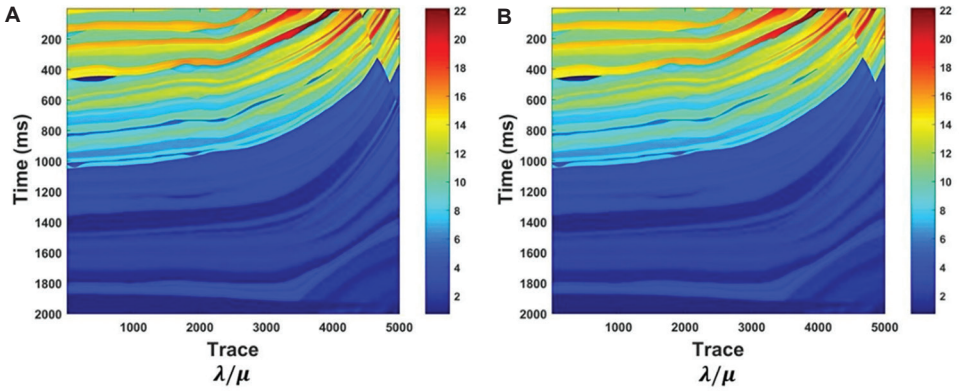

Figure 4. λ/μ inversion results. (A) The time–domain L1 horizontal constraint regularization; and (B) the two-step sub-band regularization.

method and the sub-band regularization method in more detail, this paper extracts the 1,000th trace data of the used model for single-trace analysis, as shown in Figure 8. From the single-trace inversion effect, it can be clearly seen that the single-trace inversion record obtained by the sub-band regularization method has a higher matching degree with the original data, more minor inversion error, and higher accuracy. To more intuitively demonstrate the difference in inversion performance between the time–domain L1 horizontal constraint regularization method and the two-step sub-band regularization method. Table 1 details the root mean square error (RMSE) of the inversion results obtained by these two methods.

$$RMSE = \sqrt{\frac{\sum_{i=1}^{n}(L - L_{model})^2}{n}} \quad \text{(XXI)}$$

In **Equation (XXI)**, L represents the inversion result and L_{model} represents the theoretical model of the inversion. The smaller the RMSE, the higher the inversion accuracy of this method. By comparing the data in the table, the two-step sub-band regularization method has lower RMSE in the inversion results of the three parameters compared to the

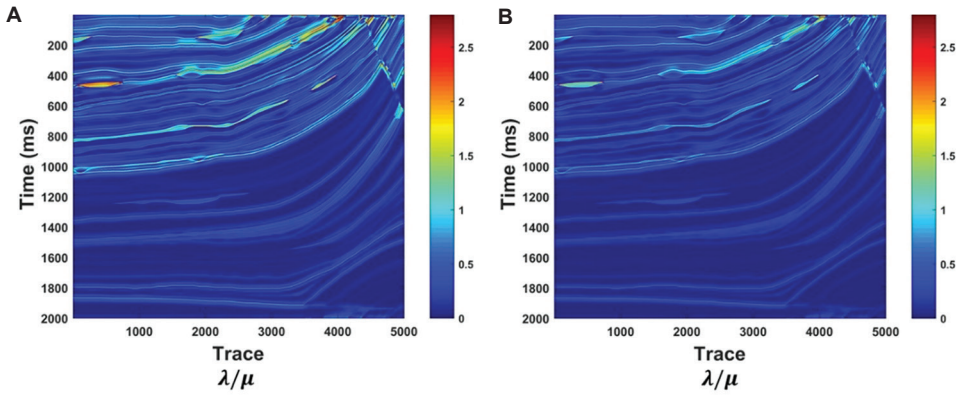

Figure 5. λ/μ inversion error. (A) The time-domain L1 horizontal constraint regularization; and (B) the two-step sub-band regularization.

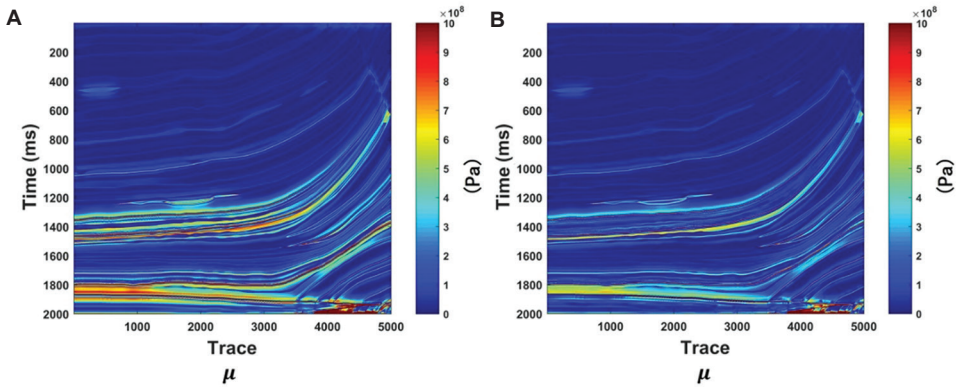

Figure 6. μ inversion error. (A) The time–domain L1 horizontal constraint regularization; and (B) the two-step sub-band regularization.

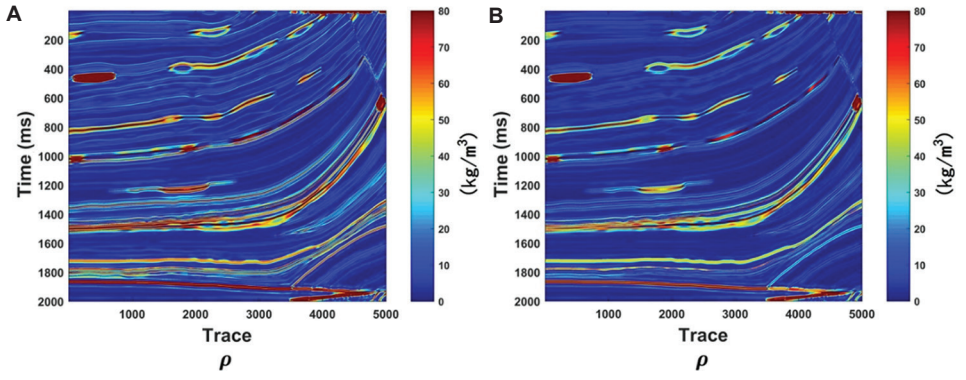

Figure 7. ρ inversion error. (A) The time-domain L1 horizontal constraint regularization; and (B) the two-step sub-band regularization.

time–domain L1 horizontal constraint method. This result fully indicates that the sub-band regularization method is superior to the time–domain L1 horizontal constraint regularization method in terms of inversion effect and can more effectively improve the inversion accuracy.

In addition, we also compared the running time of the two methods. Due to the larger computational complexity and the need for two inversions, the frequency domain method has a higher time consumption, as clearly reflected in Table 2. After multiple experimental verifications, the time consumption of the proposed method is about twice that of the L1 method in the time domain. The entire experimental paper is based on a computer processing unit, Intel (R) Xeon (R) CPU E5-2680 v4 × 2 @ 2.40GHz.

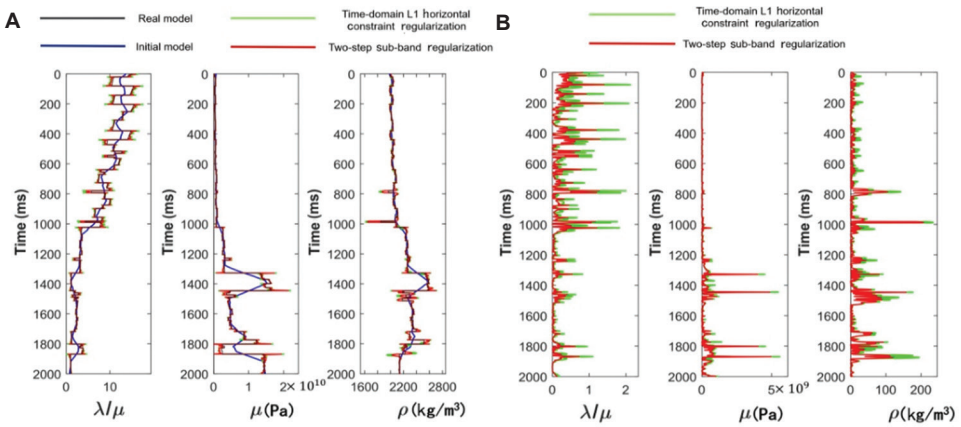

Figure 8. Single-trace data inversion results and errors. (A) Inversion results and (B) inversion result errors.

Table 1. Root mean square error comparison of 5,000 traces inversion results from different methods

Method	Root mean square error		
	λ/μ	μ (*Pa*)	ρ (*kg/m³*)
Time-domain L1 horizontal constraint regularization	0.013	1.0687×10⁷	1.0123
Two-step sub-band regularization	0.0064	0.7788×10⁷	0.6096

Table 2. Comparison of the time consumption of different methods

Method	Time	Data size
Time-domain L1 horizontal constraint regularization	12 min	5,000×2,000
Two-step sub-band regularization	26 min	5,000×2,000

To further verify the noise resistance performance of the method, a noise tolerance experiment was conducted with an additional 5dB signal-to-noise ratio (SNR) of Gaussian white noise, considering that field seismic data contain certain noise. Figure 9 shows the comparison of inversion results from different methods after the addition of noise. The analysis indicates that when the SNR is 5dB, abnormal features appeared in the inversion results, and the inversion errors of both regularization methods exhibited an increase in abnormal points. However, compared with the time–domain L1 regularization method, the proposed two-step sub-band regularization method demonstrated superior performance in terms of continuity and stability of inversion results, with more minor errors and a more uniform distribution. The experimental results confirm that the two-step sub-band regularization method can still maintain high inversion accuracy and reliability under low SNR conditions, fully highlighting the advantages of this method. It should be noted that the current method is only effective on random noise. If there is coherent noise in the data, denoising methods should be applied first for noise suppression. This is also consistent with the situation in field data inversion (where the noise after data denoising is mostly random noise).

3.2. Field data testing

To further verify the effectiveness of the method, the time–domain horizontal constraint L1 regularization method and the two-step sub-band regularization method were applied to an actual work area. These field data were from a shale gas development area in the Sichuan Basin, China. We presented some well-crossing angle stack sections. Figure 10 shows the seismic data volumes with incident angles of 12°, 24°, and 36°, respectively. The section contained 793 traces with a trace interval of 20 m and a vertical time sampling interval of 2 ms.

In the process of seismic inversion, smoothing of logging data is a key step in constructing the initial model. First, the initial model of the work area can be obtained by smoothing the logging data, as shown in Figure 11. This model provides an essential foundation for subsequent seismic data inversion.

As shown in Figures 12-14, the inversion results of fluid factors, shear modulus, and density are displayed respectively. Figures 12-14A show the results of the time–domain horizontal constraint L1 regularization method, and Figures 12-14B show those of the two-step sub-band regularization method. From the inversion results, it can be seen that compared with the time–domain horizontal constraint L1 regularization method, the two-step sub-band regularization method significantly improved the lateral continuity of inversion results. Meanwhile, the vertical resolution is effectively enhanced, and the overall performance is notably improved.

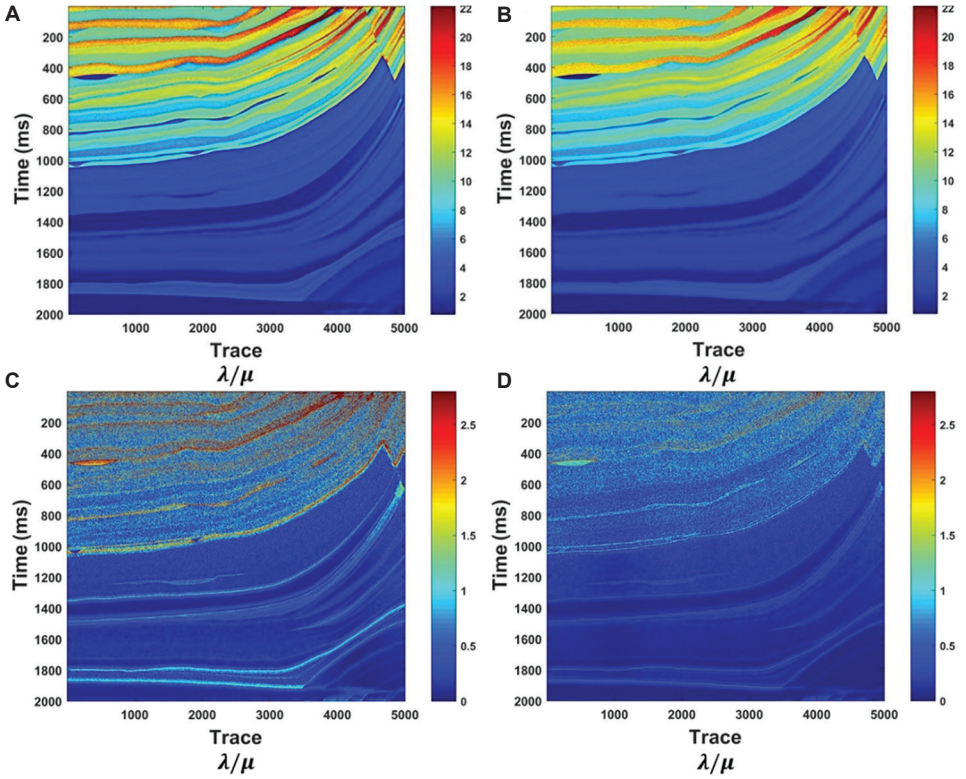

Figure 9. Inversion results and errors of fluid factors with added noise. (A) Inversion results of time–domain L1 horizontal constraint regularization; (B) inversion results of two-step sub-band regularization; (C) inversion errors of time–domain L1 horizontal constraint regularization; and (D) inversion errors of two-step sub-band regularization.

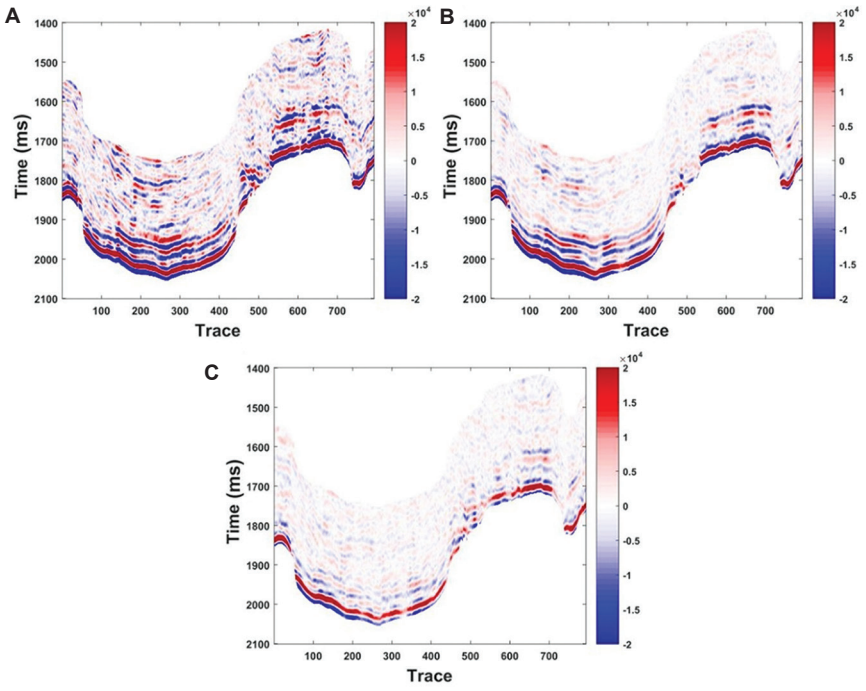

Figure 10. Angle stack section of field data. (A) 12°; (B) 24°; and (C) 36°.

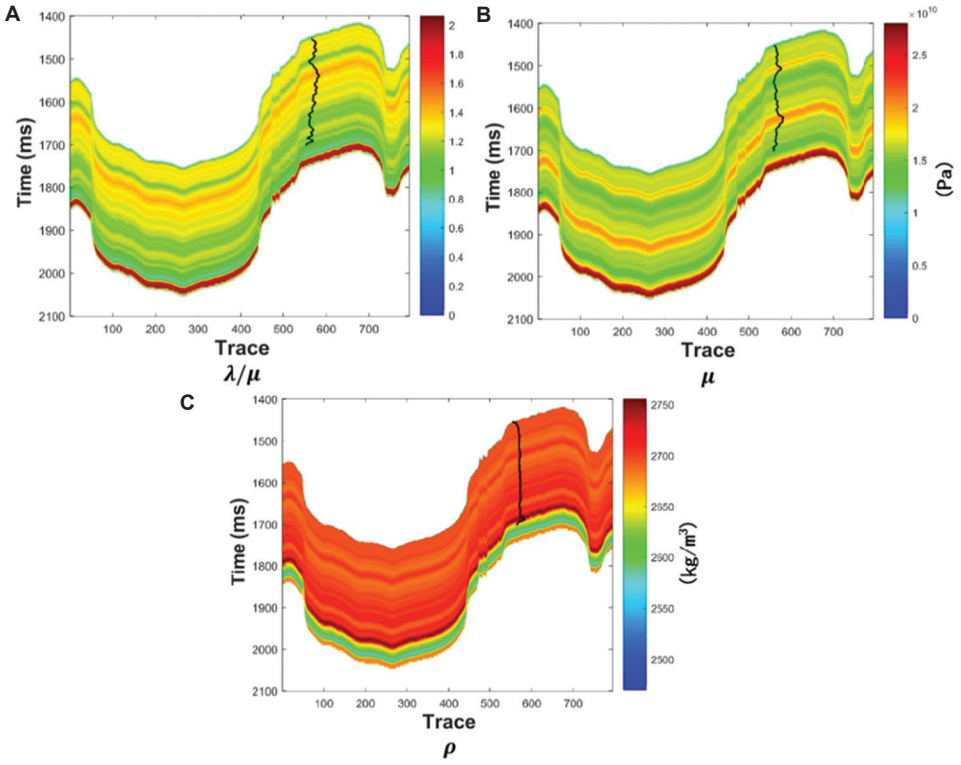

Figure 11. Initial model. (A) λ/μ.; (B) μ.; and (C) ρ.

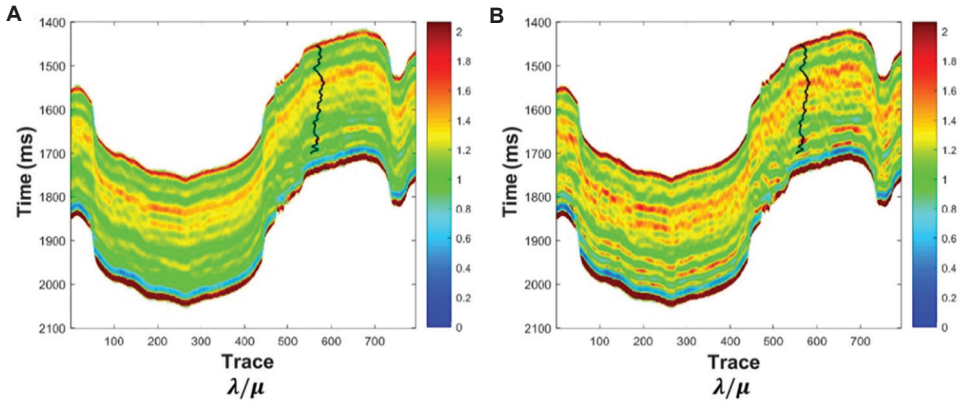

Figure 12. λ/μ inversion results. (A) The time–domain L1 horizontal constraint regularization; and (B) the two-step sub-band regularization.

To verify the reliability of the inversion results, we extracted the well-side traces and conducted a detailed comparison with the logging data. Figure 15 presents the inversion comparison results of the two methods: The black curve represents the actual logging curve, the blue curve denotes the inversion result of the time–domain horizontal constraint L1 regularization method, and the red curve stands for the inversion result of the two-step sub-band regularization method. For a more detailed comparison, Table 3 shows the correlation coefficients between the inversion results and the logging data. The results show that although the two-step sub-band regularization method achieved a limited improvement, its inversion results were closer to the logging data and exhibited higher stability. This indicates that the method can more accurately capture geological features during the inversion process, thereby providing more reliable and precise inversion results.

Regarding the relatively slight improvement effect shown in Figure 15, we speculate that it mainly stems from two reasons: first, as observed from the original seismic data, the resolution of the well-side data itself

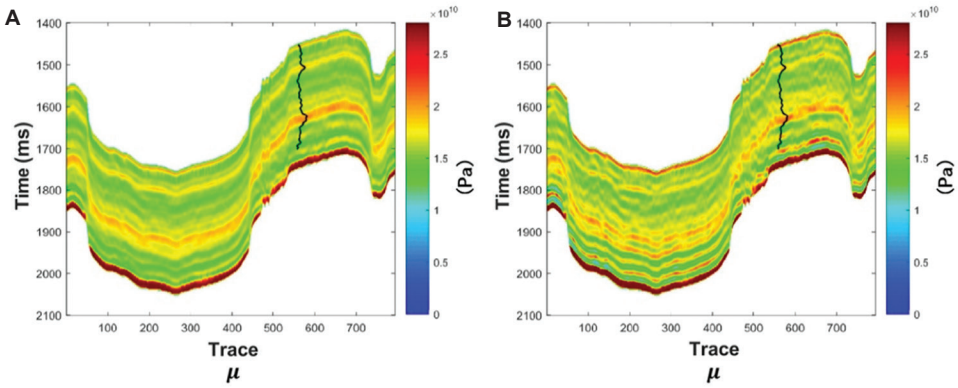

Figure 13. μ inversion results. (A) The time–domain L1 horizontal constraint regularization; and (B) the two-step sub-band regularization.

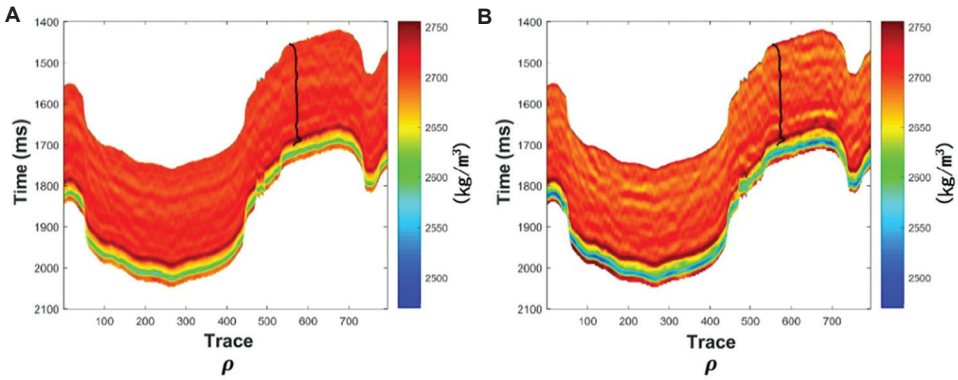

Figure 14. ρ inversion results. (A) The time–domain L1 horizontal constraint regularization; and (B) the two-step sub-band regularization.

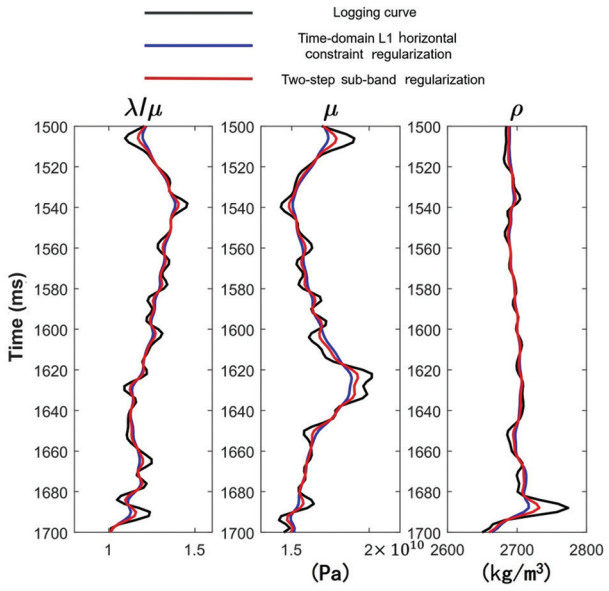

Figure 15. Comparison of well-side trace inversion results

has limitations, which to a certain extent restricts the full exertion of the performance of the proposed method; second, there is a deviation between the extracted wavelet and the real wavelet, and this factor also affects the actual inversion effect.

Table 3. Comparison of correlation coefficients between inversion results and logging data

Method	Root mean square error		
	λ/μ	μ	ρ
Time–domain L1 horizontal constraint regularization	0.6824	0.5973	0.7158
Two-step sub-band regularization	0.7456	0.6608	0.7326

4. Discussion

In response to the differences in information contained in different frequency bands of seismic data (low frequencies reflect structural outlines, while high frequencies depict detailed features), this paper groundbreakingly proposes a two-step frequency-band division regularization method. Through frequency-band division processing, geological information in different frequency bands was explicitly enhanced during inversion, avoiding information confusion caused by the unified processing

of the whole frequency band. Meanwhile, the Alternating Direction Method of Multipliers was adopted to efficiently decompose and solve the objective function, ensuring the algorithm's convergence and computational efficiency. The results of the theoretical model experiments clearly verify the significant improvement of this method in inversion accuracy and noise resistance. This fully demonstrates the scientific validity and feasibility of the frequency-band division strategy, providing a new technical approach for the accurate inversion of fluid factors.

It should be further clarified that the proposed method has certain applicable conditions and limitations. First, the data needs to meet the requirements of multi-angle pre-stack seismic data and complete logging data, ensuring the reliability of frequency domain feature extraction and initial model. The second is that the geological structure adapts to sudden changes in the lateral strata without severe fragmentation. If there are large-scale thrust structures or global fractured zones, it will destroy the frequency domain data correlation and lead to the failure of lateral constraints. The third is that fluid differences can be distinguished by λ/μ. If the fluid differences are weak or the reservoir exceeds the range of seismic frequency band identification, the advantages of the method are difficult to reflect.

Furthermore, as a core factor of geological complexity, the impact of fracture development on inversion results requires focused attention, with specific variations depending on the degree of fracture development: In areas with low-to-moderate fracture development, microfractures only slightly alter elastic parameters and the overall λ/μ remains dominated by fluid type; the proposed method can capture weak anomalies of gas-bearing fractures through high-frequency inversion. In areas with high fracture development, seismic wave scattering blurs the low-high frequency stratification characteristics in the frequency domain, and fracture fillings may obscure the fluid indication significance of λ/μ, thereby affecting inversion results. In areas with extreme fracture development, where seismic wave propagation is dominated by scattering-diffraction, the linear relationship of the forward model fails, and inversion results cannot distinguish the contributions of fluids, fractures, and karst caves, leading to the fundamental failure of the method.

5. Conclusion

This study focused on pre-stack seismic inversion methods and proposes a new fluid factor inversion method based on a two-step sub-band regularization in the frequency domain. Starting from the ill-posed problem of pre-stack seismic inversion based on the constructed fluid factor reflection coefficient formula, the study successively constructs the time–domain horizontal constraint L1 regularization and frequency-domain horizontal constraint L1 regularization methods, finally developing the two-step sub-band regularization inversion method. Theoretical model and field data verification results showed that the new method has significant advantages in vertical resolution, lateral continuity, and noise resistance, outperforming the traditional time–domain horizontal constraint L1 regularization method. By directly inverting fluid factors, this method effectively reduces cumulative errors. Combined with the frequency-domain horizontal constraint mechanism, it minimizes inversion uncertainties. Experimental verification confirms its feasibility, providing a high-precision and robust inversion tool for fluid prediction under complex geological conditions.

Finally, it is worth noting that this study still has certain limitations, which need to be further improved in subsequent work. First, the selection of current regularization parameters relies on manual experience and multiple sets of experimental trials. Although it is operable in small-scale data experiments, it will require a significant amount of time and effort when applied to actual large-scale seismic data. In subsequent research, automated methods (such as L-curve analysis or cross-validation methods) can be considered to optimize the selection of regularization parameters. Secondly, the current process of dividing high and low frequencies is very subjective. In future research, it is necessary to develop algorithms to automatically divide high and low frequencies and discuss the impact of different frequency band divisions on the inversion results.

Acknowledgments

None.

Funding

This work was supported in part by the Technology Cooperation Project of the CNPC-SWPU Innovation Alliance (2020C×020000) and in part by the Natural Science Foundation of Sichuan Province (24NSFSC0808).

Conflict of interest

The authors declare they have no competing interests.

Author contributions

Conceptualization: Peng Xiao
Formal analysis: Pang Chen
Investigation: Peng Xiao, Wangyang Xu
Methodology: Peng Xiao
Writing–original draft: Peng Zhang
Writing–review & editing: Ying Xiao

Availability of data

The data supporting the findings of this study are available from the corresponding author on reasonable request.

References

1. Smith GC, Gidlow PM. Weighted stacking for rock property estimation and detection of gas. *Geophys Prospect*. 1987;35(9):993-1014.

   doi: 10.1111/j.1365-2478.1987.tb00856.x

2. Goodway B, Chen T, Downton J. Improved AVO fluid detection and lithology discrimination using lame petrophysical parameters; "λρ, μρ, λμ fluid stack", From P and S inversions. *SEG Ann Meet*. 1997;22:183-186.

   doi: 10.1190/1.1885795

3. Connolly P. Elastic impedance. *Lead Edge*. 1999; 18(4):438-438.

   doi: 10.1190/1.1438307

4. Smith GC. *The Fluid Factor Angle and the Crossplot Angle*. *SEG Annual Meeting*. United States: Society of Exploration Geophysicists; 2003.

   doi: 10.1190/1.1817679

5. Peng ZM, Li YL, Wu SH, He ZH, Zhou YJ. Discriminating gas and water using multi-angle extended elastic impedance inversion in carbonate reservoirs. *Chin J Geophys*. 2008;51(3):881-885.

   doi: 10.1002/cjg2.1253

6. Zheng JJ, Yin XY, Zhang GZ. Fluid factor analysis and the construction of the new fluid factor. *Prog Geophys*. 2011;26(2):579-587.

   doi: 10.3969/j.issn.1004-2903.2011.02.024

7. Zong Z, Yin X, Wu G. Direct inversion for a fluid factor and its application in heterogeneous reservoirs. *Geophys Prospect*. 2013;61(5):998-1005.

   doi: 10.1111/1365-2478.12038

8. Yin X, Zong Z, Wu G. Research on seismic fluid identification driven by rock physics. *Sci China Earth Sci*. 2015;58(2):159-171.

   doi: 10.1007/s11430-014-4992-3

9. Li C, Zhang JM, Zhu ZY. Direct inversion method for fluid factor in deep reservoirs. *Petrol Geophys Prospect*. 2017;56(6):827-834.

   doi: 10.3969/j.issn.1000-1441.2017.06.008

10. Jiang Z, Xiong Y. Seismic inversion for fluid bulk modulus based on elastic impedance. *J Appl Geophys*. 2019;169:74-84.

    doi: 10.1016/j.jappgeo.2019.06.013

11. Liu C, Ghosh DP, Salim AMA, Chow WS. A new fluid factor and its application using a deep learning approach. *Geophys Prospect*. 2019;67(1):140-149.

    doi: 10.1111/1365-2478.12712

12. Li K, Yin XY, Zong ZY. Facies-constrained prestack seismic probabilistic inversion driven by rock physics. *Sci China Earth Sci*. 2020;50(6):832-854.

    doi: 10.1007/s11430-019-9578-1

13. Farfour M, Castagna JP. A new expression for fluid factor using AVO intercept and gradient. *Soc Explor Geophys*. 2021;9(1):267-271.

    doi: 10.1190/segam2021-3575102.1

14. Wu HB, Wu RX, Zhang PS, Huang Y, Dong S. Combined fluid factor and brittleness index inversion for coal-measure gas reservoies. *Geophys Prospect*. 2022;70(4):751-764.

    doi: 10.1111/1365-2478.13172

15. Zhou L, Liao JP, Liu XY, Wang P, Guo YN, Li JY. A high resolution inversion method for fluid factor with dynamic dry-rock VP/VS ratio squared. *Petrol Sci*. 2023;20(5):2822-2834.

    doi: 10.1016/j.petsci.2023.09.015

16. Ruyi Z, Huan W, Yongqiang M, Jianhua T, Chao H, Maoqiang Z. Fluid factor inversion based on *Q* elastic impedance. *Geophys Prospect Petrol*. 2024;63(4):826-832.

    doi: 10.12431/issn.1000-1441.2024.63.04.011

17. Pan F, Li SJ, Qin DW, *et al*. Direct inversion method for fluid factor and anisotropic parameters in VTI media. *Oil Geophys Prospect*. 2024;59(4):875-886.

    doi: 10.13810/j.cnki.issn.1000-7210.2024.04.025

18. Tikhonov AN. On the stability of inverse problems. *Dokl Akad Nauk Sssr*. 1943;39(5):195-198.

19. Tikhonov AN. Solution of incorrectly formulated problems and the regularization method. *Sov Math Dok*. 1963;4:1035-1038.

20. Rudin LI, Osher S, Fatemi E. Nonlinear total variation based noise removal algorithm. *Phys D Non Phenom*. 1992;60(4):259-268.

    doi: 10.1016/0167-2789(92)90242-F

21. Zou H, Hastie T. Regularization and variable selection via the elastic net. *J Roy Statis Soc*. 2005;67(2):301-301.

    doi: 10.1111/j.1467-9868.2005.00503.x

22. Gholami A. Nonlinear multichannel impedance inversion by total-variation regularization. *Geophysics*. 2015;80(5):217-224.

    doi: 10.1190/geo2015-0004.1

23. Ruixue S, Liguo H, Eryan S, *et al*. Dual-parameter shaping regularized full waveform inversion in frequency domain. *Glob Geol*. 2015;18(4):258-262.

    doi: 10.3969/j.issn.1673-9736.2015.04.09

24. Mousavi SM, Langston CA, Horton SP. Automatic microseismic denoising and onset detection using the synchrosqueezed continuous wavelet transform. *Geophysics*. 2016;81(4):341-355.

doi: 10.1190/geo2015-0598.1

25. Pan S, Chen Y, Yin C, Gou Q, Zhang D. Prestack inversion method with ATpV regularization based on reweighted L1. *J S Petrol Univ Sci Technol*. 2024;46(3):13-26.

doi: 10.11885/j.issn.1674-5086.2022.08.20.02

26. Wang D, Zhang YM, Niu C, *et al*. The optimization of sensitive fluid factor removing the effect of porosity and its application to hydrocarbon detection. *Geophys Geochem Explor*. 2021;45(6):1402-1408.

doi: 10.11720/wtyht.2021.1364

Appendix

A. Forward equation derivation

To accurately extract key parameters from seismic data, it is necessary to establish the connection between the seismic data and the parameters to be inverted using the reflection coefficient equation. Taking density ρ as an example, the reflection coefficient of density ρ in seismic data can be approximately expressed as **Equation (A1)**:

$$R_{\_\rho} = \frac{\rho_{i+1} - \rho_i}{\rho_{i+1} + \rho_i} \approx \frac{1}{2}\Delta ln(\rho) = \frac{1}{2}[ln(\rho_{i+1}) - ln(\rho_i)] \tag{A1}$$

Let L_i be the natural logarithm of density ρ, and $L_i = ln(\rho)$ **(Equation [A2])**:

$$R_{\_\rho} \approx \frac{1}{2}(L_{i+1} - L_i) \tag{A2}$$

And $R_{\_\rho}$ can be expressed in matrix form **(Equation [A3])**:

$$R_{\_\rho} = \frac{1}{2}DL \tag{A3}$$

Where L is the natural logarithm of density and D is the difference matrix.

The construction of the seismic inversion objective function is based on the mathematical foundation of the convolution model. In this process, the wavelet convolution kernel matrix is first introduced to transform the wavelet convolution operation in seismic data into linear algebraic operations **(Equation [A4])**:

$$S = W \cdot R \tag{A4}$$

By using the angle-dependent wavelet matrix W(θ), the angle-dependent forward seismic record S(θ) can be expressed as **Equation [A5]**:

$$\begin{bmatrix} S(\theta) \\ \vdots \\ S(\theta_M) \end{bmatrix} = \frac{1}{2}\begin{bmatrix} W(\theta_1) & & \\ & \ddots & \\ & & W(\theta_M) \end{bmatrix}\begin{bmatrix} a(\theta_1) & b(\theta_1) & c(\theta_1) \\ \vdots & \vdots & \vdots \\ a(\theta_M) & b(\theta_M) & c(\theta_M) \end{bmatrix}\begin{bmatrix} -1 & 1 & 0 & 0 & \cdots & 0 \\ 0 & -1 & 1 & 0 & \cdots & 0 \\ \ddots & \ddots & \ddots & \ddots & \ddots & \vdots \\ 0 & 0 & \cdots & \cdots & -1 & 1 \end{bmatrix}\begin{bmatrix} L_{\lambda/\mu} \\ L_\mu \\ L_\rho \end{bmatrix} \tag{A5}$$

Where $a(\theta_i)$, $b(\theta_i)$, and $c(\theta_i)$ are all diagonal matrices, and the matrix composed of these three diagonal matrices is defined as B. Then, the forward modeling equation based on the linear approximation formula can be abbreviated as **Equation [A6]**:

$$S = WBDL = AL \tag{A6}$$

Where $A = WBD$.

B. An example of a sensitivity analysis comparison figure for regularization parameters

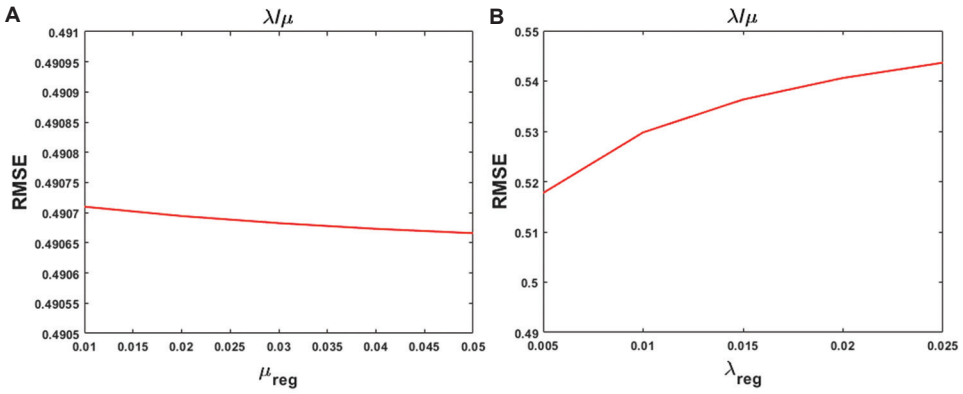

Figure A1. λ/μ inversion results. (A) The impact of μ_{reg} on the inversion results of λ/μ. (B) The impact of r_{reg} on the inversion results of λ/μ. Abbreviation: RMSE: Root mean square error.